



HAL
open science

Steering of magnetotactic bacterial microrobots by focusing magnetic field for targeted pathogen killing

Changyou Chen, Linjie Chen, Pingping Wang, Long-Fei Wu, Tao Song

► To cite this version:

Changyou Chen, Linjie Chen, Pingping Wang, Long-Fei Wu, Tao Song. Steering of magnetotactic bacterial microrobots by focusing magnetic field for targeted pathogen killing. *Journal of Magnetism and Magnetic Materials*, 2019, 479, pp.74-83. 10.1016/j.jmmm.2019.02.004 . hal-02333896

HAL Id: hal-02333896

<https://amu.hal.science/hal-02333896>

Submitted on 10 Feb 2020

HAL is a multi-disciplinary open access archive for the deposit and dissemination of scientific research documents, whether they are published or not. The documents may come from teaching and research institutions in France or abroad, or from public or private research centers.

L'archive ouverte pluridisciplinaire **HAL**, est destinée au dépôt et à la diffusion de documents scientifiques de niveau recherche, publiés ou non, émanant des établissements d'enseignement et de recherche français ou étrangers, des laboratoires publics ou privés.



Distributed under a Creative Commons Attribution - NonCommercial - NoDerivatives 4.0 International License

Steering of magnetotactic bacterial microrobots by focusing magnetic field for targeted pathogen killing

Changyou Chen ^{a,c}, Linjie Chen ^{a,b}, Pingping Wang ^{a,c}, Long-Fei Wu ^{c,d}, and Tao Song ^{a,b,c,*}

1

2 ^a Beijing Key Laboratory of Bioelectromagnetism, Institute of Electrical Engineering, Chinese
3 Academy of Sciences, Beijing 100190, China.

4 ^b University of Chinese Academy of Sciences, Beijing 100049, China.

5 ^c France-China International Laboratory of Evolution and Development of Magnetotactic
6 Multicellular Organisms, Beijing, China.

7 ^d Aix Marseille Univ, CNRS, LCB, Marseille, France.

8

9 * **Corresponding author at:** Beijing Key Laboratory of Bioelectromagnetism, Institute of
10 Electrical Engineering, Chinese Academy of Sciences, Beijing 100190, PR China.

11 **E-mail address:** songtao@mail.iee.ac.cn (T. Song).

12 **Permanent address:** No. 6 Bei'er Tiao Zhongguancun HaiDian, Beijing, 100190, P. R. China

13 **Tel:** 86-10-82547164

14 **Fax:** 86-10-82547164

15

1 **Abstract**

2 Targeted steering of magnetotactic bacterial microrobots is a growing tendency for
3 their various biomedical applications. However, real-time monitoring during their
4 movements and targeted cell killing in specific locations remain challenging. Here,
5 we steered bacterial microrobots to target and attach to *Staphylococcus aureus* that
6 was subsequently killed in a magnetic target device, which can realize guiding,
7 mixing, and killing for targeted therapy. The generated focusing magnetic field was
8 applied to magnetotactic bacterial microrobots, and the realizability of control
9 strategies was analyzed. We successfully guided magnetotactic bacterial microrobots
10 in microfluidic chips without real-time monitoring of their location. After mixing with
11 microrobots under a rotating magnetic field for their attachment, the pathogen was
12 killed under a swinging magnetic field. These results suggest that targeted therapy
13 with these microrobots by using a magnetic target device is a promising approach.

14

15 **Keywords:** Magnetotactic bacteria; Microrobot; Focusing magnetic field; Targeted
16 Therapy; *Staphylococcus aureus*

17

18 **1. Introduction**

19 Numerous advances in the development of microrobots with various architectures
20 have been described[1-3]. Some microrobots with a targeting ability are essential for
21 the noninvasive targeted therapy of diseases, such as tumor or infection in deep
22 tissues[4, 5]. Magnetotactic bacteria show potential as actuators for the construction
23 of microrobots with targeting abilities owing to their special characteristics. They are
24 a unique group of bacteria that swim along magnetic field lines because of their
25 intracellular magnetic crystals called magnetosomes [6-9]. Some of these bacteria are
26 autotrophic which can supply energy by themselves; and their motile speed can reach
27 300 $\mu\text{m/s}$ [10, 11]. As a result, the motile direction of magnetotactic bacterial
28 microrobots can be easily controlled by magnetic fields. These characteristics endow
29 them with many biomedical applications, for example, pathogen target [12], cargo
30 delivery [13, 14], and drug transport [15-17].

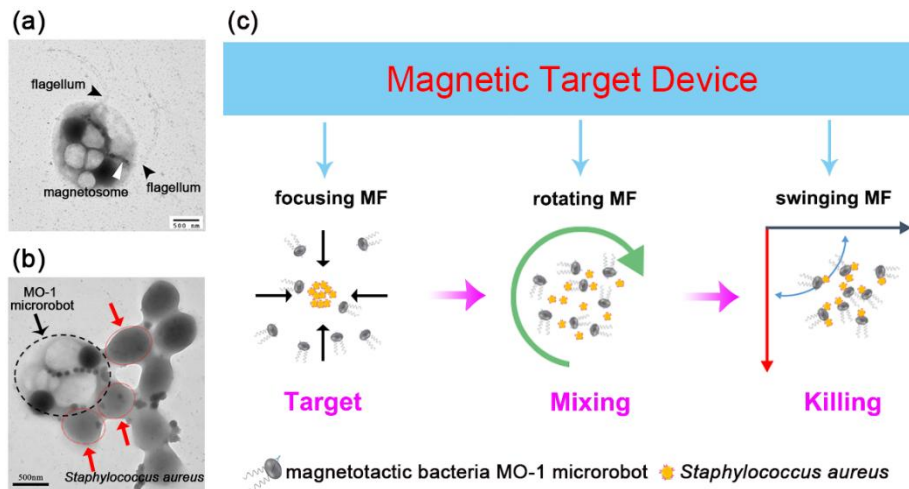
31 One of the key points in these applications is the magnetic control of
32 magnetotactic bacteria to reach a target. In general, a static magnetic field adjusted in
33 real time can provide directions for magnetotactic bacteria because they can sense
34 geomagnetic fields. Thus, guiding these bacteria is easily achieved via a static
35 magnetic field if the swimming route and location of magnetotactic bacteria could be
36 tracked in real time in a microfluidic chip under a microscope [18]. However,
37 real-time monitoring of the location of magnetotactic bacteria is difficult in
38 complicated environments, such as the human body, despite the availability of

1 information about the pattern of a flowing passageway. Thus, a simple magnetic field
2 cannot be adjusted momentarily. Therefore, three groups of Maxwell coils were used.
3 Each group of Maxwell coils consist of two identical coils with a certain distance and
4 could produce two magnetic fields of opposite direction, respectively. The two
5 magnetic fields were superposed to form a gradient magnetic field. The three groups
6 of Maxwell coils were modulated by a time-sequencing program to produce a
7 focusing magnetic field equivalent to a magnetic field whose directions in the space
8 point to or are oriented away from the focusing center. This focusing magnetic field
9 can guide magnetotactic bacteria and induce their aggregation in a precise location
10 [19]. On the basis of Maxwell coil groups, the introduction of multiple focusing
11 points within the motion path was proposed to navigate magnetotactic bacteria to
12 successively reach the targets [19, 20]. Maxwell coil method with a given control
13 tactics is independent of the location of magnetotactic bacteria and can consequently
14 avoid difficulties in detecting the position of these bacteria *in vivo* at all times [21].
15 Therefore, how to set and optimize focusing points in the complicated channels needs
16 to be further investigated.

17 Another key point in targeted therapy is the execution of functions when
18 magnetotactic bacterial microrobots arrive at the target. Magnetotactic bacteria can be
19 constructed as drug-carrier microrobots [15, 16]. Applying an alternating magnetic
20 field to induce magnetic hyperthermia of magnetotactic bacteria is an alternative [22,
21 23]. However, these applications generally needs two sets of independent devices that
22 can generate guiding and alternating magnetic fields respectively. The heat effect may
23 also damage the surrounding healthy cells in clinical applications. Thus, real-time
24 temperature measurement is needed. However, detecting and regulating the
25 temperature at deep target locations are difficult when applying an alternating
26 magnetic field.

27 In view of these challenges, the navigation of magnetotactic bacterial microrobots
28 without real-time monitoring and targeted killing by applying different magnetic
29 fields in an integrated device may be the new trends. In previous reports, we
30 demonstrated that magneto-ovoid strain MO-1, a kind of magnetotactic bacteria, are
31 coated by a MO-1 specific antibody to be microrobots and then can attach to
32 *Staphylococcus aureus* (*S. aureus*) that was killed by applying a swinging magnetic
33 field (Fig. 1a, b) [24, 25]. The device used to produce a swinging magnetic field is
34 similar to that used to generate a focusing magnetic field. In the present study, we
35 conducted the targeted killing of *S. aureus* by using magnetotactic bacterial
36 microrobots in a magnetic target device, which could produce focusing, rotating, and
37 swinging magnetic fields (Fig. 1c). We optimized the control strategy and investigated
38 the possibility of targeted navigation and aggregation of magnetotactic bacteria in the
39 microchannel of microfluidic chip within the magnetic target device. Once the

1 magnetotactic bacterial microrobots arrived at the target, rotating magnetic field
 2 assisted the mixing of microrobots and *S. aureus* for their attachment, and then
 3 swinging magnetic fields generated by the device under different control circuits were
 4 applied to kill *S. aureus*.



5
 6 **Fig. 1.** Schematic of targeted killing of *Staphylococcus aureus* by magnetotactic bacterial
 7 microrobots. (a) Magnetotactic bacteria (MTB) MO-1 with a chain of magnetosome and two
 8 bundles of flagella [24]. (b) Attachment of magnetotactic bacteria MO-1 to *S. aureus* [24].
 9 Antibody-coated magnetotactic bacteria MO-1 (microrobots) could attach to *S. aureus* via the
 10 affinity between MO-1 specific antibody and Protein A expressed in the surface of *S. aureus*.
 11 Black arrows noted MO-1 microrobot and red arrows indicated *Staphylococcus aureus*. (c) MO-1
 12 microrobots was first navigated to the target by focusing magnetic field (MF), mixed with *S.*
 13 *aureus* under rotating MF for their attachment, and then killed *S. aureus* under swinging MF.

14 2. Theory

15 We expect that a focusing magnetic field B could be applied to steer
 16 magnetotactic bacteria to reach the target area without knowing the location
 17 information. A plane focusing magnetic field is produced through two orthogonal coil
 18 groups. One group called x-coil produces an x-directional gradient magnetic field,
 19 while the other group named y-coil generates a y-directional gradient magnetic field.
 20 X- and y-directional gradient magnetic fields are alternately produced, thereby
 21 generating a focusing magnetic field in a time scale, as shown in Fig. 2.

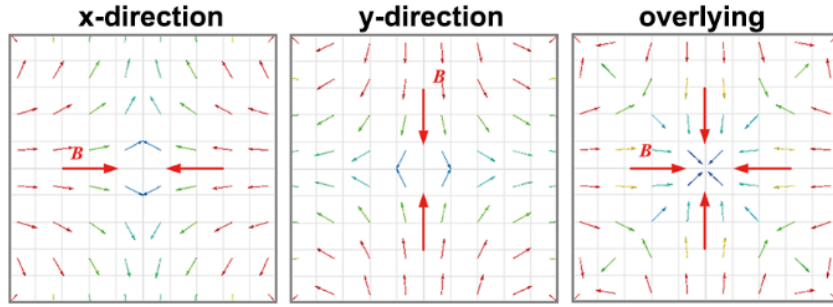


Fig. 2. Principle for production of focusing magnetic field. X- and y-directional gradient magnetic fields are alternately produced, finally generating a focusing magnetic field. Red, yellow, green and blue note the magnitude of magnetic field in descending order.

In a plane, the width of the microchannel in a microfluidic chip is ignored. The microchannel height is not considered either in a two dimension as microchannel height in each microfluidic chip is same and does not affect the theoretical results. Then the shape of the microchannel in a microfluidic chip can be expressed by the following function/curve: $y = f(x)$. Here, we assumed that the friction coefficient between the microchannel wall and magnetotactic bacteria is large enough. We could obtain the following theories:

Theorem The necessary and sufficient condition for guiding magnetotactic bacteria from the initial point P_0 to destination P_1 (focusing center) when an applied focusing magnetic field is generated by independently using x- and y-coils is that the function $y = f(x)$ for the microchannel shape is a monotone function.

When the function $y = f(x)$ for the microchannel shape is a monotone function, we can easily prove that the focusing magnetic field can navigate magnetotactic bacteria (Fig. 3a). X-coils produce an x-directional gradient magnetic field that steer magnetotactic bacteria to swim in the x-direction, and y-coils generate a y-directional gradient magnetic field that control their motion in the y-direction. Therefore, magnetotactic bacteria could be guided finally to the focusing center through alternated usage of x- and y-coils.

If the function $y = f(x)$ is not a monotone function, then two cases will be analyzed. For the case where the function $y = f(x)$ is a monodrome but not a monotone function (Fig. 3b), a point of x_0 corresponding to maximum or minimum value y_0 can be observed. At the two sides of x_0 , the direction of the focusing magnetic field that navigates magnetotactic bacteria to P_1 is the opposite. So it is impossible to achieve the aggregation of magnetotactic bacteria. For the case where the function $y = f(x)$ is multivalued, x-directional magnetic field is balanced at an x point corresponding to multivalued y (y_1 and y_2) (Fig. 3c). As a result, the focusing magnetic field cannot navigate magnetotactic bacteria to the destination (focusing center) either.

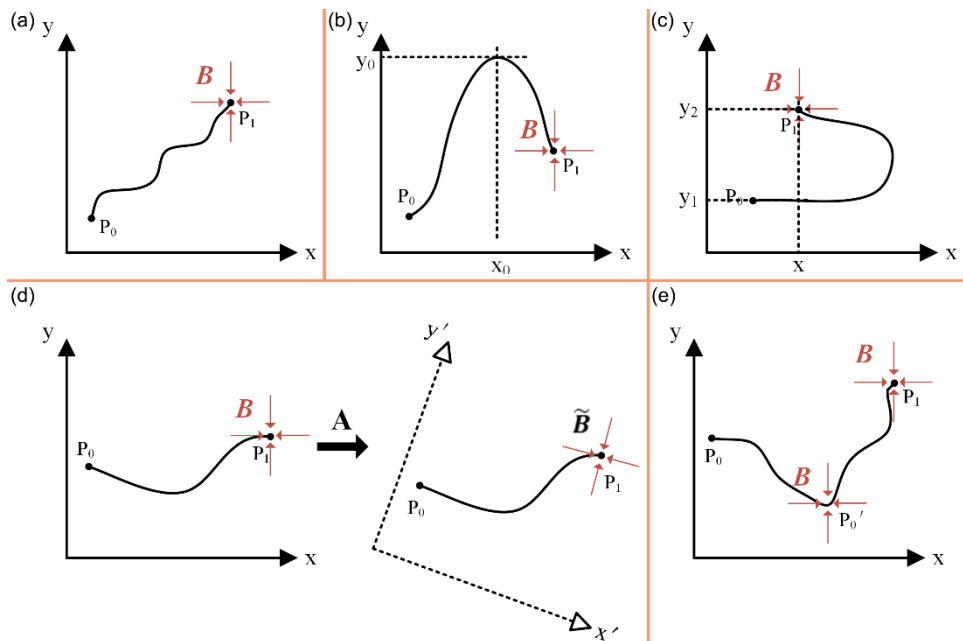
Corollary 1 The necessary and sufficient condition for guiding magnetotactic bacteria

1 from the initial point P_0 to destination P_1 (focusing center) under the control of the
 2 focusing magnetic field produced by the combination of x- and y-coils is the presence
 3 of a Cartesian coordinate transformation \mathbf{A} that makes the function $y = f(x)$
 4 transform to a monotone function $\tilde{y} = \tilde{f}(\tilde{x})$.

5 At the moment, applying a focusing magnetic field $\tilde{\mathbf{B}}$ on the microchannel can
 6 be achieved by combining x- and y-coils, as shown in Fig. 3d.

7 **Corollary 2** Finite points that make the subsection of the function $y = f(x)$
 8 monotone are present. Thus, the application of a focusing magnetic field successively
 9 on these points could steer magnetotactic bacteria.

10 Thus, the method of applying a focusing magnetic field can be found from the
 11 theorem (Fig. 3e).



12
 13 **Fig. 3.** Effect of microchannel shape on the control of magnetotactic bacteria under the focusing
 14 magnetic field. (a) A monotone function for a microchannel shape. (b) A non-monotone but
 15 monodrome function for a microchannel shape. It generally has a point of x_0 corresponding to
 16 maximum or minimum value y_0 . (c) The multivalued microchannel function where some x points
 17 correspond to multivalued y (y_1 and y_2). (d) The non-monotone microchannel function could be
 18 transformed to a monotone function by a Cartesian coordinate transformation \mathbf{A} . (e) Finite points
 19 make the subsection of the microchannel function monotone.

20 3. Material and methods

21 3.1. Design and fabrication of magnetic target device

22 A magnetic target device consisting of power supplies, magnetic field coils, a
 23 control circuit, and a control program was designed and fabricated, as shown in Fig.
 24 4a. Two power supplies (P_1 and P_2) (model number: DH1765-5, Beijing Dahua Radio

1 Instrument co. LTD, China) provide current for magnetic field coils. The magnetic
2 field coils were designed by using Maxwell (Ansoft Inc., PA, USA), and was
3 fabricated by ourselves. Currents in coils were adjusted through the control program
4 according to the requirement. The control program was compiled in a Microsoft
5 Visual Studio (community 2010) using C++ scripting language. The control circuit
6 was established by solid-state relays whose states were set by the control program
7 through the on–off output of the data acquisition card; the switchover of solid-state
8 relays modulates the current state. According to the size of the objective table of an
9 inverted microscope (IX70, Olympus co., Japan), we designed magnetic field coils
10 that consist of two orthogonal coil groups, and these coils can be fixed on the
11 objective table (Fig. 4b, c). Each coil group contains two identical coils placed in
12 parallel: one group called x-coil (x_1 and x_2 coils) produces an x-directional gradient
13 magnetic field, and the other group named y-coil (y_1 - and y_2 -coils) generates a
14 y-directional gradient magnetic field.

15 The control program was used to choose the corresponding circuit. P_1 and P_2
16 supplied currents for the x_1 - and x_2 -coils, respectively. We set the currents in the x_1 -
17 and x_2 -coils with the same magnitude in opposite directions. The x_1 - and x_2 -coils
18 produced a gradient magnetic field in the x-axis pointing toward the geometric center of
19 x-coil, and this phenomenon maintained a period of $T/2$. Then, the control program was
20 utilized to choose another circuit. As a result, P_1 and P_2 provided currents for the y_1 -
21 and y_2 -coils, respectively, with the same magnitude in opposite directions. A gradient
22 magnetic field in the y-axis pointing toward the geometric center of the magnetic field
23 coils was also generated by the y_1 - and y_2 -coils. This phenomenon sustains another
24 period of $T/2$. Within a period of T , gradient magnetic fields in the x- and y-axes
25 overlaid, thereby generating a focusing magnetic field (Fig. 2). We implemented the
26 focusing magnetic field on a time scale by continuing the repetition of this process.

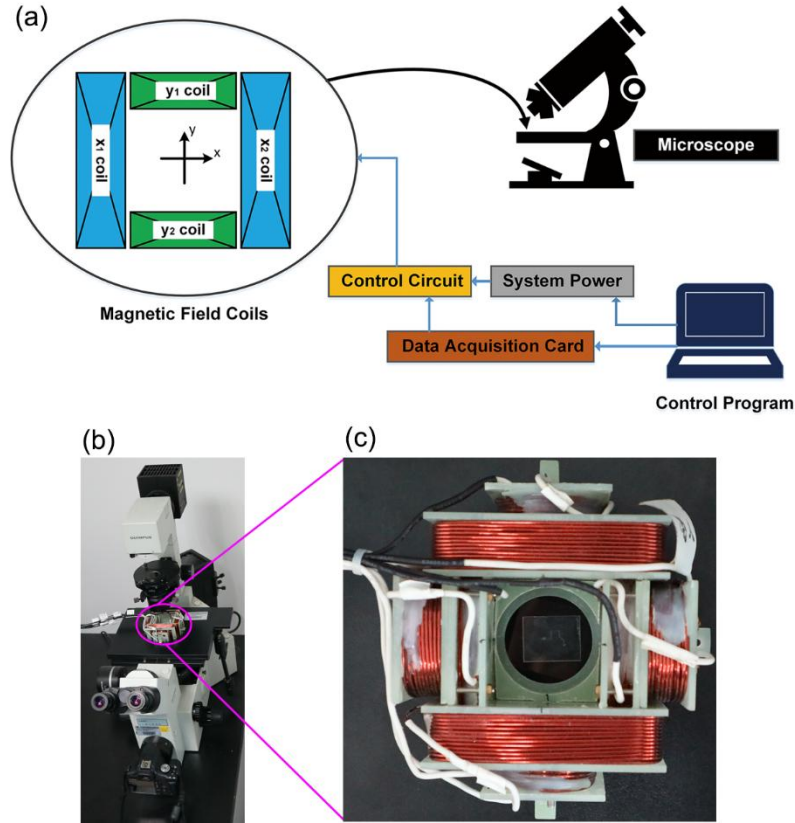


Fig. 4. Fabrication of a magnetic target device. (a) Schematic of magnetic target device. The device mainly consists of power supplies, magnetic field coils, control circuit as well as control program. (b) The embedded magnetic field coils into the objective table. (c) The magnetic field coils. The coils consist of two orthogonal coil groups

The location of the focusing center of focusing magnetic field could be adjusted by changing the current magnitude of each coil in the x- or y-coils to steer magnetotactic bacteria flexibly. The amplitude of the magnetic field on the axis of a rectangular coil is described in Eq. (1) [26]:

$$B = \frac{\mu_0 I a b}{4\pi \sqrt{h^2 + \frac{a^2 + b^2}{4}}} \left(\frac{1}{h^2 + \frac{a^2}{4}} + \frac{1}{h^2 + \frac{b^2}{4}} \right), \quad (1)$$

where B is the amplitude of the magnetic field on the axis of a rectangular coil, a and b are the two rectangular side lengths, h is the distance from one point on the axis of a rectangular coil to the center of the rectangular coil, μ_0 is the permeability of the vacuum, and I is the current. In addition, (1) the currents in a coaxial coil pair comprising I_1 and I_2 coils are I_1 and I_2 , respectively; (2) the distance between the coil pair is $2h$; and (3) the distance covered by the focusing center diverging from the central point of the coaxial coil is δ . The distances from the focusing center to I_1 and I_2 coils are $h + \delta$ and $h - \delta$, respectively. The offset of the gradient magnetic field produced by I_1 and I_2 coils can be determined by the following:

$$\begin{aligned}
& \frac{\mu_0 n I_1 a b}{4\pi \sqrt{(h+\delta)^2 + \frac{a^2+b^2}{4}}} \left(\frac{1}{(h+\delta)^2 + \frac{a^2}{4}} + \frac{1}{(h+\delta)^2 + \frac{b^2}{4}} \right) \\
& = \frac{\mu_0 n I_2 a b}{4\pi \sqrt{(h-\delta)^2 + \frac{a^2+b^2}{4}}} \left(\frac{1}{(h-\delta)^2 + \frac{a^2}{4}} + \frac{1}{(h-\delta)^2 + \frac{b^2}{4}} \right)
\end{aligned} \tag{2}$$

I_1 and I_2 in the two coils satisfy the following equation:

$$\frac{I_1}{I_2} = \frac{\sqrt{(h+\delta)^2 + \frac{a^2+b^2}{4}}}{\sqrt{(h-\delta)^2 + \frac{a^2+b^2}{4}}} \cdot \frac{\frac{1}{(h-\delta)^2 + \frac{a^2}{4}} + \frac{1}{(h-\delta)^2 + \frac{b^2}{4}}}{\frac{1}{(h+\delta)^2 + \frac{a^2}{4}} + \frac{1}{(h+\delta)^2 + \frac{b^2}{4}}} \tag{3}$$

For the square coil, a is equal to b , and $a^2/4$ is equal to A . Eq. (3) can be written as follows [21]:

$$\frac{I_1}{I_2} = \frac{\sqrt{(h+\delta)^2 + 2A}}{\sqrt{(h-\delta)^2 + 2A}} \cdot \frac{(h+\delta)^2 + A}{(h-\delta)^2 + A} \tag{4}$$

Therefore, two sets of currents satisfying Eq. (4) can cause the location of the focusing center to diverge a distance of δ from the geometric center of the coaxial coil.

In addition to the focusing magnetic field, rotating and swinging magnetic fields can be generated using the magnetic target device fabricated here. In the generation of rotating and swinging magnetic fields, P_1 provides currents with the same magnitude and direction for the x_1 - and x_2 -coils by choosing the corresponding circuit under the setting of the control program, thereby creating a magnetic field in the x -axis. P_2 also supplies currents for the y_1 - and y_2 -coils, thereby producing the other magnetic field in the y -axis. A rotating magnetic field can be generated in a discrete mode by controlling the power supply and circuit in accordance with the program. When P_1 and P_2 yield currents according to a certain frequency, the magnetic target device can generate a swinging magnetic field with the corresponding frequency in a space enclosed by magnetic field coils.

3.2. Fabrication of microfluidic chip

To test our analyses, we developed three types of glass microfluidic chips: Z-chip with a monotonic channel, U-chip with a nonmonotonic channel, and M-chip with a piecewise monotonic channel. Each type of glass microfluidic chips was characterized by a width of 200 μm and a height 20 μm , and comprised sample and target holes with 400 μm in diameter. The three chips were fabricated by photomasking, lithography

1 exposure, film development, chrome removal, etching, chip cutting and drilling, and
2 hot compaction. In brief, a photomask was prepared using a PET film according to the
3 designed shape of the microfluidic chip. A Cr plate was aligned to the mask and
4 exposed using a lithography machine. Afterward, the Cr plate was placed with its light
5 rubber oriented in a forward direction and imaged in 0.5% NaOH for 40 s to rinse the
6 part of the imaged light rubber. The Cr plate was fixed with water for 1 min. After
7 drying, its light rubber was positioned in a forward direction in an oven at 110 °C for
8 15 min to solidify the remanent light rubber. After cooling to room temperature, the
9 Cr plate with its photoresist surface upward was enched in Cr removal solution to
10 remove naked Cr by shaking gently for 40 s. A glass substrate with a shape of a
11 transparent channel was formed after water cleaning and drying. Adhesive tapes were
12 pasted to the back and edge of the substrate as a protective layer, and the pasted
13 substrate with the channel side upward was etched by immersing it in an etchant at
14 40 °C with slow shaking. The etched substrate was rinsed in water, and the adhesive
15 tapes were removed. Then, the glass substrate was punched by a straight-handle twist
16 drill in the micropores. Finally, the glass substrate was bound with coverslips at a high
17 temperature. The chips can be placed on the center of the magnetic field coils and
18 fixed to the objective table of the microscope.

19 3.3. Preparation of magnetotactic bacteria MO-1 and *S. aureus*

20 Magneto-ovoid strain MO-1 was grown in EMS2 medium at room temperature
21 and collected until the exponential phase was reached [10]. A permanent magnetic
22 block made of Nd-Fe-B was placed around 2 mL Eppendorf tubes containing MO-1
23 solution to enrich the MO-1 cells. To determine the cell concentration, some solution
24 containing the enriched MO-1 cells was mixed with 4% formaldehyde to let MO-1
25 cells lose the motility. Then the number of MO-1 was counted using a hemacytometer
26 under a microscope and the original concentration of MO-1 was further determined.

27 *S. aureus* (ATCC25923) was grown on blood LB agar plates (Land Bridge
28 Technology Co., Ltd., Beijing, China) in an incubator at 37 °C. Bacterial cells were
29 harvested and suspended in normal saline buffer containing 0.9% NaCl. Their
30 concentration was measured through conventional plate counting.

31 3.4. Navigation of magnetotactic bacteria MO-1 in microfluidic chips

32 Navigation experiments were carried out in the three types of microfluidic chips.
33 1.5×10^7 MO-1 was injected into the sample hole of microfluidic chips. Through the
34 adjustment of electric current in the *x*- and *y*-axes, the focusing magnetic field was
35 produced to cover the chips, and its focusing center was set. The time sequence of the
36 focusing magnetic field was set to 10 s. Considering that MO-1 is a North-Seeking
37 magnetotactic bacterium which preferentially swims parallel to the magnetic field, we

1 used the focusing magnetic field equivalent to a magnetic field whose directions in
2 the space point to the focusing center for navigation. When a focusing magnetic field
3 was applied, the movement of MO-1 was monitored under the brightfield of the
4 microscope (objective: 40×; light source: mercury lamp) to validate the aggregation
5 effect and not to provide positional information for magnetic field control. The videos
6 are recorded by using a camera (EOS 500D, Canon Inc., Japan) connected to the
7 microscope. The relative position between the magnetic field coils and the
8 microfluidic chip remained unchanged when the objective table of the microscope
9 was shifted because the chip, the magnetic field coils, and the objective table were
10 fixed to one another.

11 3.5. Targeted killing of *S. aureus* by magnetotactic bacterial microrobots

12 *S. aureus* was subjected to targeted killing in M-chip. Magnetotactic bacterial
13 microrobots were first constructed according to our previous study [24]. Briefly,
14 magnetotactic bacteria MO-1 was first incubated with rabbit anti-MO-1 polyclonal
15 antibodies for 30 min at room temperature; rabbit anti-MO-1 polyclonal antibodies
16 specifically react with MO-1 surface antigens to construct MO-1 microrobots; after
17 that, MO-1 microrobots of good activity were enriched by a permanent magnetic
18 block for the following experiment. Then, 1.5×10^7 microrobots were injected into the
19 sample hole, and 1.5×10^6 *S. aureus* was simultaneously injected into the target hole.
20 When the microrobots were guided to arrive at the target hole, a rotating magnetic
21 field was exerted to induce the intensive mixing between *S. aureus* and MO-1
22 microrobots. Then, *S. aureus* was incubated for 30 min at room temperature for their
23 attachment to MO-1 microrobots through antibody-protein A interaction [23, 24]. A
24 swinging magnetic field with an intensity of 10 mT and a frequency of 2 Hz was
25 applied for 40 min. After the application of swinging magnetic field, the *S. aureus*
26 solution in the target hole was diluted by 100-fold, and 50 μ l dilution was spread on
27 blood LB agar plates. The number of *S. aureus* clones was counted after the plates
28 were incubated overnight in a thermostatic incubator at 37 °C. Meanwhile, the case in
29 the absence of the swinging magnetic field was used as its control group. Besides, *S.*
30 *aureus* alone group (SA) and the simple mixture group (SA + MO-1) where MO-1
31 cells which is not coated by a MO-1 specific antibody were also guided to the target
32 hole of M-chip containing *S. aureus* were also performed in the presence and absence
33 of swinging magnetic field.

34 3.6 Statistical analysis

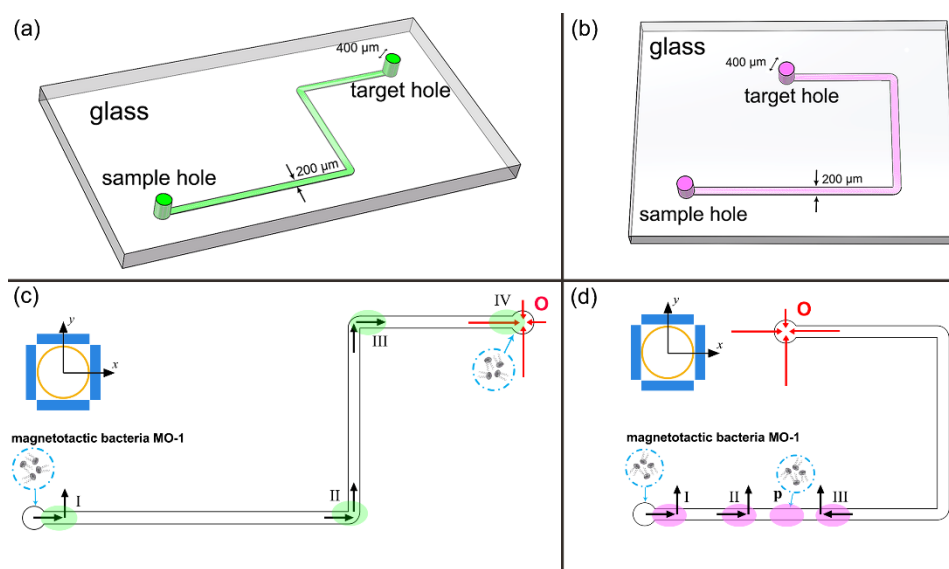
35 Data for *S. aureus* clone was acquired by averaging clone number of three plates
36 in each experiment. Data were expressed as mean \pm standard deviation (SD). Each
37 killing experiment was independently performed thrice. Student's *t*-test was applied to

1 compare the difference. Differences with a P value of < 0.05 were considered
 2 significant in the statistical test.

3 **4. Results**

4 *4.1. Movement of magnetotactic bacteria MO-1 in Z- and U-chips under the control of* 5 *focusing magnetic field*

6 The control effect of the focusing magnetic field on magnetotactic bacteria MO-1
 7 was first observed in the Z- (Fig. 5a) and U-chips (Fig. 5b). The Z-chip channel can
 8 be expressed as a monotone function, whereas the U-chip channel can be expressed as
 9 a nonmonotonic and multivalued function. According to theory, the magnetotactic
 10 bacteria would aggregate at the target hole in the Z-chip (Fig. 5c) and not in the
 11 U-chip (Fig. 5d) when the focusing center was set on the target holes of the two chips.

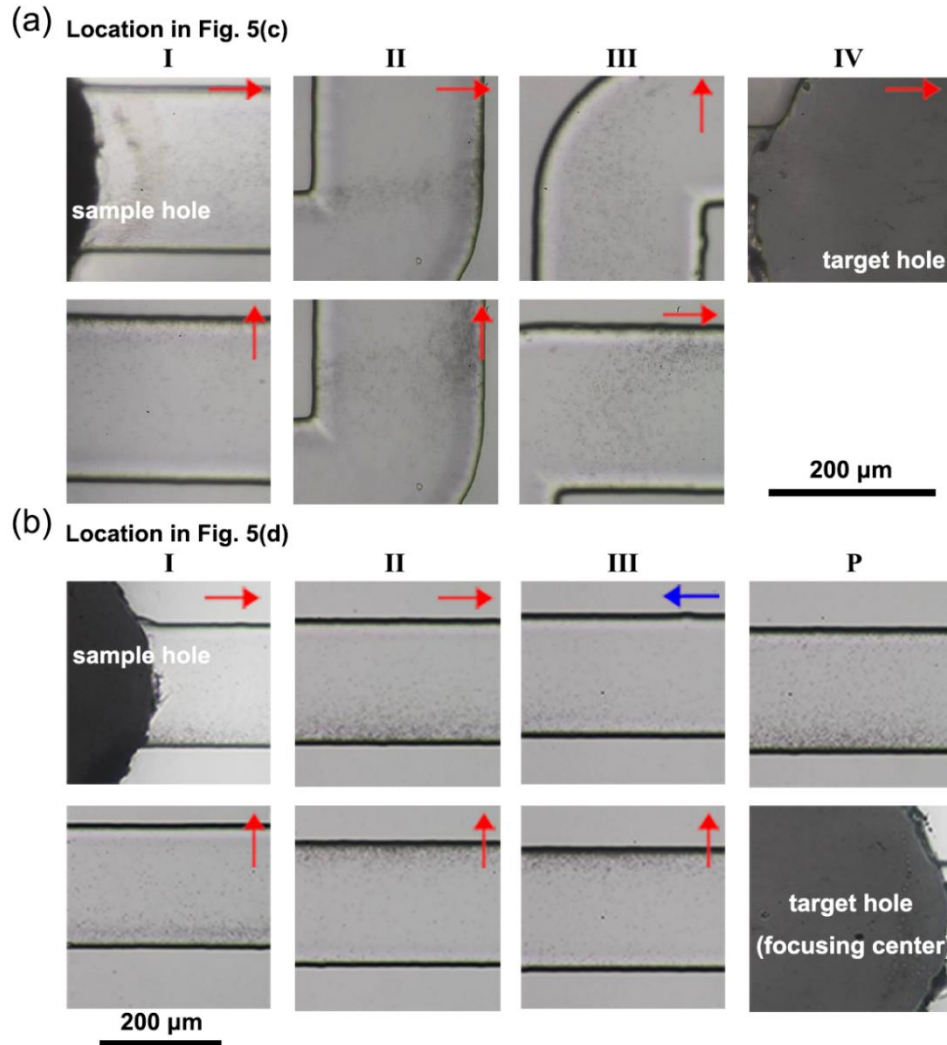


12
 13 **Fig. 5.** Movement analysis of magnetotactic bacteria MO-1 under the control of focusing
 14 magnetic field in Z-chip and U-chip. (a) Z-chip. (b) U-chip. (c) Schematic movement of
 15 magnetotactic bacteria MO-1 in Z-chip when the focusing center **O** (four red counter-arrows) was
 16 fixed directly on the target hole. (d) Schematic movement of magnetotactic bacteria MO-1 in
 17 U-chip when the focusing center **O** (four red counter-arrows) was fixed directly on the target hole.
 18 Black arrows in the microchannel in (c) and (d) note the direction of focusing magnetic field
 19 magnetotactic bacteria MO-1 felt during their movement.

20 Fig. 6a shows the movement of MO-1 in the Z-chip under the control of the
 21 focusing magnetic field. MO-1 cells in the sample hole initially sensed the rightward
 22 direction of the focusing magnetic field at site I located in Fig. 5c and consequently
 23 swam away from the sample hole along this magnetic field (Fig. 6a). After 5 s in the
 24 rightward magnetic field, the direction of the focusing magnetic field changed upward,
 25 which caused MO-1 aggregation in the wall of the microfluidic chip (Fig. 6a). After 5

1 s in the upward magnetic field, the direction of the focusing magnetic field was
2 rightward again, which guided the MO-1 cells to move continuously. When the MO-1
3 cells arrived at the first turn shown in site II, the change in the magnetic field
4 direction from rightward to upward guided them to pass the turn, and the focusing
5 magnetic field continuously assisted these cells. The same scenario was observed in
6 the second turn in site III, that is, MO-1 passed through the turn. Finally,
7 magnetotactic bacteria MO-1 reached the target hole (site IV) controlled by the
8 focusing magnetic field (Fig. 6a).

9 Fig. 6b illustrates the movement of MO-1 cells from the sample hole of the
10 U-chip under the focusing magnetic field. The MO-1 cells at the sample hole initially
11 perceived the rightward direction of the focusing magnetic field. As a result, they
12 swam away from the sample hole for 5 s at site I of the U-chip, as shown in Figs. 5d
13 and 6b. As the direction of the focusing magnetic field changed upward, the MO-1
14 cells moved to and aggregated on the channel wall at site I. Under the control of the
15 focusing magnetic field, the MO-1 cells continuously swam in the channel, such as at
16 site II, until they reached the **P** site (Figs. 5d and 6b). At the **P** site, the MO-1 cells
17 perceived only the gradient magnetic field in the y-direction because the x-directional
18 magnetic field was balanced dynamically. Therefore, they swam back and forth at the
19 **P** site (site III) (Fig. 6b). The target hole (focusing center) over the **P** site was
20 observed by moving the microscopic objective table (Fig. 6b). We did not find any
21 magnetotactic bacteria in the target hole, suggesting that the bacteria in the U-chip
22 could not reach the target hole. Hence, our experimental results in the Z- and U-chips
23 were consistent with the theorem.



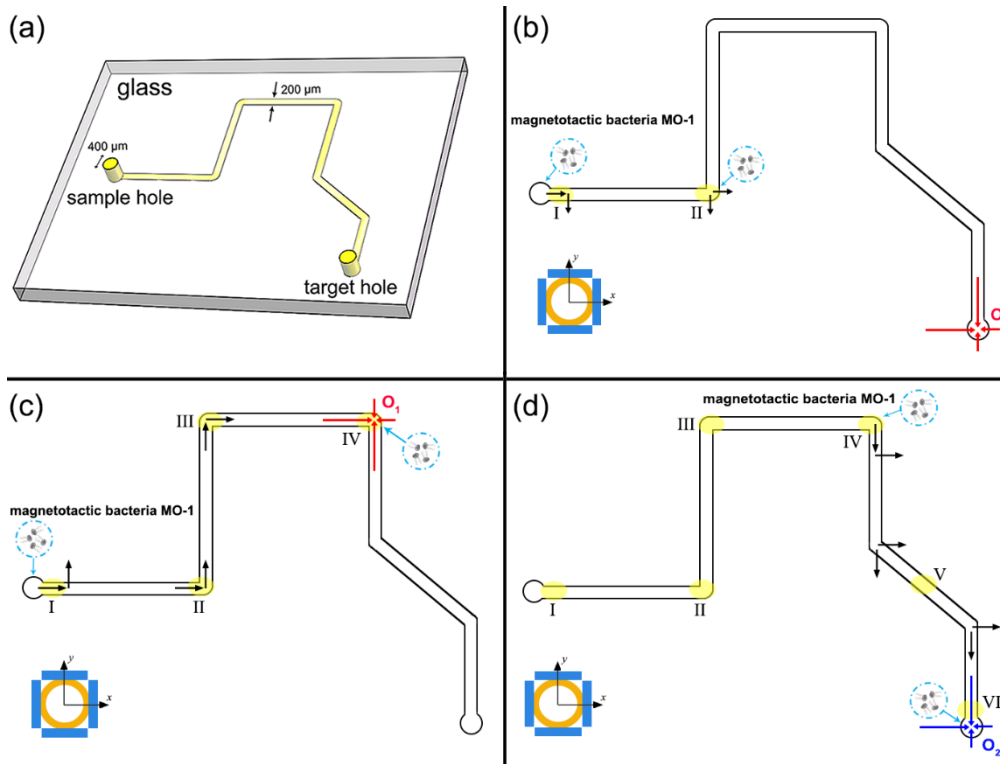
1

2 **Fig. 6.** Swimming of magnetotactic bacteria MO-1 under the control of focusing magnetic field in
 3 Z- and U-chips. (a) Movement of MO-1 microrobots in the Z-chip. Robot images shows their
 4 movements in different location in sites of Fig. 5c under the control of focusing magnetic field. (b)
 5 Movement of MO-1 microrobots in U-chip. Robot images shows their movements in different
 6 location in sites of Fig. 5d under the control of focusing magnetic field. Red and blue arrows note
 7 the direction of focusing magnetic field. Two videos are available as additional material.

8 *4.2. Guiding magnetotactic bacteria MO-1 in M-chip by using the focusing magnetic*
 9 *field*

10 The schematic of M-chip fabrication is shown in Fig. 7a. In an orthogonal plane
 11 coordinate system, the channel of the M-chip was expressed as a nonmonotonic
 12 function. If the focusing center **O** of the focusing magnetic field was set directly on
 13 the target hole, then the magnetotactic bacteria aggregated at site II (Fig. 7b) and
 14 cannot arrive at the target hole. According to Corollary 2, the shape of the M-chip
 15 could be segmented as a piecewise continuous function by point IV. Thus, we chose
 16 point IV as the first focusing center (**O₁**) (Fig. 7c) and then set the center on the target

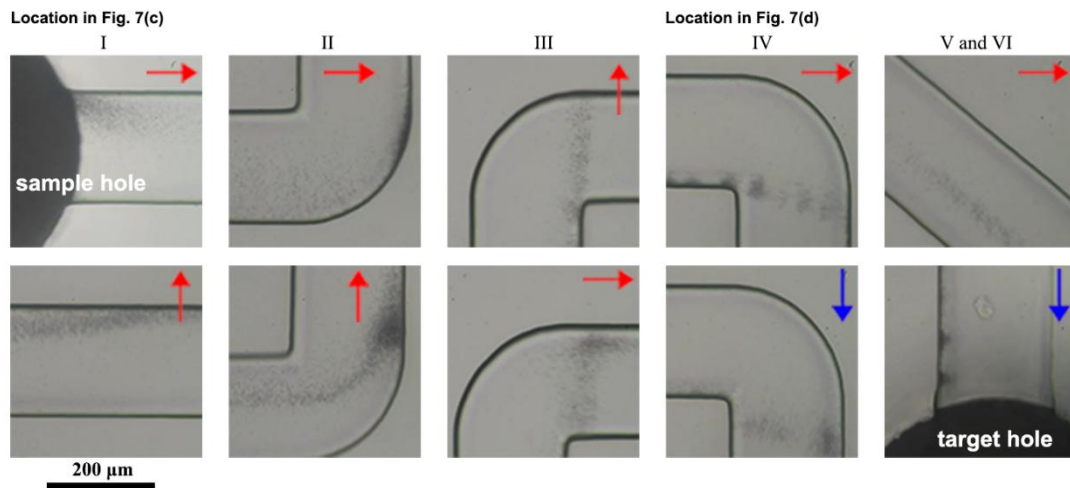
1 hole (O_2) after the magnetotactic bacteria arrived at the first focusing center (Fig. 7d).



2

3 **Fig. 7.** Movement analysis of magnetotactic bacteria MO-1 under control of focusing magnetic
 4 field in microfluidic M-chip. (a) Microfluidic M-chip. (b) Schematic of movement of magnetotactic
 5 bacteria MO-1 in M-chip when the focusing center O was directly set on the target hole. (c)
 6 Schematic movement of magnetotactic bacteria MO-1 in M-chip from site I to site IV when the
 7 focusing center O_1 was first set on site IV. (d) Movement of magnetotactic bacteria MO-1 in
 8 M-chip from site IV to the target hole when the focusing center O_2 was then set on target hole.
 9 Black arrows in the microchannel note the direction of focusing magnetic field in a time sequence
 10 that magnetotactic bacteria exposed to during their movement.

11 The experimental demonstration of MO-1 movement under the control of the
 12 focusing magnetic field is shown in Fig. 8. Similar to the condition in Z-chip, MO-1
 13 cells were controlled to swim at site I, moved across the two turns at sites II and III,
 14 and arrived at the first focusing center O_1 at site IV (Fig. 8). If the focusing center was
 15 maintained at site IV, then the magnetotactic bacteria persistently aggregated. Then,
 16 we changed the focusing center to the target hole. As a result, the direction of the
 17 magnetic field in the y -axis was downward (Fig. 7d). MO-1 cells consequently swam
 18 downward shown as blue arrows at site IV (Fig. 8), went through the curve channel at
 19 site V, and finally arrived at the target hole at site VI (Fig. 8). These results
 20 demonstrated that the magnetotactic bacteria could be steered in complex flows by
 21 choosing and setting some specific points under the focusing magnetic field.



1

2

3

4

5

6

7

Fig. 8. Swimming of Magnetotactic bacteria MO-1 in M-chip under the control of focusing magnetic field. Microrobots MO-1 images depict the detailed status of magnetotactic bacteria MO-1 movement under the focusing magnetic field control. Their locations are corresponding to the site I, II, III, IV in Fig. 7c, V and VI in Fig. 7d, respectively. Red and blue arrows note the direction of focusing magnetic field. A video is available as additional material.

4.3. Targeted killing of *S. aureus* by magnetotactic bacteria MO-1 microrobots

8

9

10

11

12

13

14

15

16

17

18

19

20

21

22

23

24

25

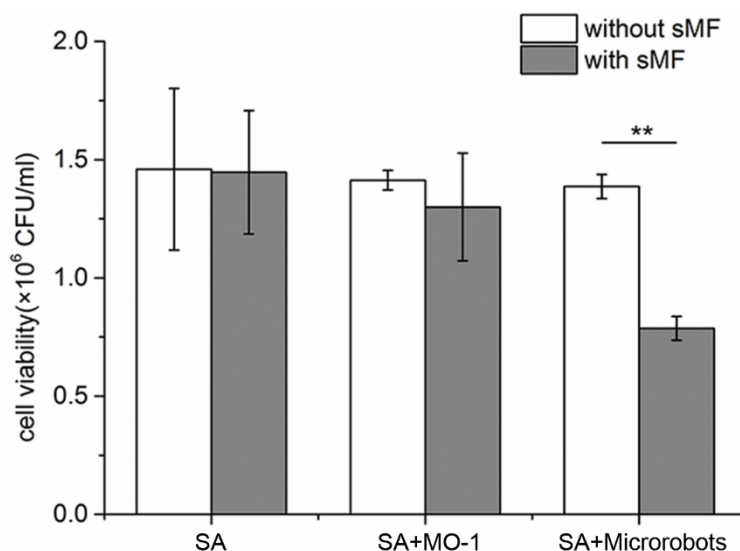
26

27

28

The guidance provided by the focusing magnetic field demonstrated the potential of the magnetotactic bacteria for targeted therapy, even in deep tissues. We previously showed that MO-1 can kill *S. aureus* under either alternating [23] or swinging magnetic fields [25] and that bacterial MO-1 microrobots can be fabricated by coating MO-1 cells with their antibodies [24]. Basing from these findings, we used MO-1 microrobots to target *S. aureus* under the control of the focusing magnetic field and eradicated this pathogen under a swinging magnetic field. In M-chip, 1.5×10^7 MO-1 microrobots and 1.5×10^6 *S. aureus* were injected into the sample and target holes, respectively. The MO-1 microrobots successfully arrived at the target hole in M-chip after about 80 s when the focusing magnetic field was applied by the magnetic target device. A rotating magnetic field (1 mT) was exerted to induce an intensive mixing between MO-1 microrobots and *S. aureus* for their attachment. A swinging magnetic field with a frequency of 2 Hz and an intensity of 10 mT was subsequently applied for 40 min after the MO-1 microrobots conjugated to *S. aureus*. As shown in Fig. S1 in the supplementary material, the union body swung due to the oscillation of MO-1 microrobots along with swinging magnetic field (black ellipses). As a result, *S. aureus* attached to MO-1 microrobots was driven by the motion of the microrobots and consequently swung (shown as red dashed ellipses in Fig. S1 in the supplementary material). Then, the effect of the swinging magnetic field on *S. aureus* was evaluated (Fig. 9). When the MO-1 microrobots conjugated to *S. aureus*, the applied swinging magnetic field induced a significant decrease in *S. aureus* viability ($P < 0.01$).

1 Conversely, the swinging magnetic field could not kill *S. aureus* in the simple mixture
2 or in the solution containing *S. aureus* only. These results were consistent with our
3 previous findings [18, 25].



4

5 **Fig. 9.** Targeted killing of *S. aureus* by magnetotactic bacteria MO-1 microrobots. The
6 suspensions of *S. aureus* alone (SA), simple mixture (SA + MO-1) and the conjugated form that
7 MO-1 microrobots combined to *S. aureus* (SA + microrobots) were exposed to a swinging
8 magnetic field (sMF: 2 Hz, 10 mT) for 40 min. Then the number of CFU for *S. aureus* was counted
9 to quantify the cell viability. ** $P < 0.01$, $n=3$.

10 5. Discussion

11 Steering of magnetotactic bacterial microrobots to the target area is an important
12 step for the targeted killing of harmful cells. In this work, strategies to control
13 magnetotactic bacterial microrobots under a focusing magnetic field was analyzed,
14 and an integrative targeted killing of *S. aureus* was verified in a microfluidic chip. In a
15 two dimensional space, a focusing magnetic field can be generated via a simple
16 method of applying currents to the x- and y-coils simultaneously [27]. The focusing
17 magnetic field used in the present study was generated in a time-sequencing manner
18 with the fabricated device (Fig. 4). Compared with the simultaneous application of a
19 gradient magnetic field, the time-sequencing manner is more propitious for
20 magnetotactic bacteria to overcome the restraint of the pipe wall and subsequently
21 aggregate [20].

22 To overcome the influence of tortuous channels, we confirmed that the application
23 of focusing centers on specific points to steer magnetotactic bacteria was feasible. This
24 approach did not require real-time imaging and monitoring, and importantly, the
25 focusing center can be set in a small range to navigate microrobots and not necessarily
26 restricted to specific points. This trait may play a critical role especially when a

1 vascular shape may be obtained incompletely. Although our analyses and experiments
2 were carried out in two dimensional space, the case in three dimension is similar. In
3 general, acquiring a vascular shape in the human body is feasible by means of some
4 techniques, including magnetic resonance imaging [28, 29], computed tomography
5 [30], and angiography [31]. In a three dimensional environment, the guidance of
6 magnetotactic bacterial microrobots could also be achieved if three dimensional
7 channels are content with the similar monotonic functions (i.e. the projections of three
8 dimensional channels on the three planes of XYZ coordinate system are all monotonic
9 functions.). In this case, the focusing center can be set directly on the targeted hole, and
10 the gradient magnetic fields along x-, y- and z-axes are applied in a time-sequencing
11 way to guide magnetotactic bacterial microrobots. If they're more complicated
12 channels, for example the vascular network, we could also steer magnetotactic bacterial
13 microrobots in a way similar to Corollary 2. We can first identify a series of specific
14 points which are used as focusing centers and then the blood vessel could be divided
15 into many segments. After that, magnetotactic bacterial microrobots could be steered to
16 reach each specific point by applying a time-sequencing gradient magnetic field along
17 x-, y- and z-axes and finally arrive at the target. Moreover, the time for changing the
18 focusing center should also be considered during the guiding of magnetotactic bacterial
19 microrobots. In the study, the focusing center could be changed quickly by microscope.
20 When in the invisible case, we are able to acquire the path length of a channel by
21 imaging; and then the time to arrive at the given focusing center for microrobots could
22 be estimated as the velocity of magnetotactic bacterial robot is known. Considering
23 other factors(i.e. blood flow, bacteria individual difference, curve of the actual path),
24 we may set up a suitable time for bacterial microrobots to reach the focusing center and
25 then change to the next one.

26 As for three kind of microfluidic chips, the walls of the channel are straight,
27 which does not trap the motile of bacterial microrobots. But the friction coefficient of
28 microchannel is supposed to be large enough in our analysis. If the friction coefficient
29 is very small and the time sequence of the focusing magnetic field sustains slightly
30 longer, the steering of the magnetotactic bacteria or their microrobots to aggregate
31 might also be realized. However, the accumulation of most bacteria or microrobots
32 could not be achieved in this case. In addition to magnetotaxis, magnetotactic bacteria
33 also have the aerotaxis that they are able to sense the oxygen concentration and swim
34 toward the direction of low oxygen. Since deep area of tumor is a hypoxic region due to
35 the consumption of oxygen by rapidly growing tumor cells, the hypoxic status could
36 also assist MTB to guide tumor, which is complementary with magnetotaxis [17]. Other
37 electron acceptors and chemicals in the blood should also be considered when steering
38 magnetotactic bacteria.

39 As the next step, killing target cells is the ultimate goal. Previously, we have

1 performed the killing experiments by using magnetotactic bacteria MO-1 under the
2 swinging magnetic field and calculated the mechanical force, which decreased the
3 viability of *S. aureus* [25]. In the present study, the used guiding magnetic field coils
4 (Fig. 4c) was also able to produce the swing magnetic field which was similar to the
5 results by Chen et al [18]. The swinging of MO-1 microrobots with the swinging
6 magnetic field was also found here. This result suggests that a mechanical force was
7 particularly exerted on *S. aureus*, which was then killed. These experiments also
8 suggested that the integration of target navigation and therapy was essential for
9 applications involving magnetotactic bacteria. We also aimed to address this issue in
10 the study. On the one hand, focusing, rotating, and swinging magnetic fields were
11 produced in one system by using different control programs and circuits. It should be
12 noted that the steering strategy is different. The present study proposed the controlling
13 method which does not need a real time monitoring, whereas the steering was
14 performed under a microscope in the literature by Chen et al[18]. In the complex
15 vascular network, the presented steering strategy may be more advantageous. On the
16 other hand, the flow of targeted killing pathogens *in vivo* with magnetotactic bacterial
17 microrobots and magnetic fields was simulated by completely conducting target
18 aggregation, mixing, and targeted killing in one microfluidic chip.

19 **6. Conclusions**

20 In the study, we reported the targeted aggregation of magnetotactic bacterial
21 microrobots by using a focusing magnetic field to avoid difficulty in real-time
22 monitoring and targeted therapy for killing *S. aureus*. The focusing magnetic field was
23 generated in a time-sequencing manner within the magnetic target device fabricated in
24 the study. The strategy of focusing magnetic field was feasible in steering of
25 magnetotactic bacterial microrobots. Finally, we successfully decreased *S. aureus*
26 viability by using magnetotactic bacteria MO-1 microrobots under the control of
27 focusing, rotating, and swinging magnetic fields generated in the magnetic target
28 device. The combination of focusing magnetic field and controllable magnetotactic
29 bacteria in the magnetic target device showed potential for targeted killing and drug
30 delivery. However, effects from pulsating blood flow, red blood cells, friction on the
31 control of magnetotactic bacterial microrobots and the safety of magnetotactic bacteria
32 in human need further investigations for the future application.

33 **Acknowledgements**

34 We thank Dr. Haiying Shen (National Center for Nanoscience and Technology of China)
35 and Xiaofei Zhang (Wenhao Co., Ltd., Suzhou, China) for help to the fabrication of

1 microfluidic chip.

2 **Funding**

3 This work was supported by the National Key Research and Development Program of
4 China (Grant NO. 2017YFC0108501), the National Youth Foundation of China (Grant
5 NO. 31300689) and the National Foundation of China (Grant NO. 81871488).

6 **Supplementary data**

7 Supplementary data associated with this article can be found, in the online version.

8 **References**

- 9 [1] L. Schwarz, M. Medina-Sánchez, O.G. Schmidt, Hybrid BioMicromotors, *Appl.*
10 *Phys. Rev.* 4 (2017) 031301.
- 11 [2] H. Ceylan, J. Giltinan, K. Kozielski, M. Sitti, Mobile microrobots for
12 bioengineering applications, *Lab Chip*, 17 (2017) 1705-1724.
- 13 [3] L. Ricotti, B. Trimmer, A.W. Feinberg, R. Raman, K.K. Parker, R. Bashir, M. Sitti,
14 S. Martel, P. Dario, A. Menciassi, Biohybrid actuators for robotics: A review of
15 devices actuated by living cells, *Sci. Robot.* 2 (2017).
- 16 [4] K. Belharet, D. Folio, A. Ferreira, Simulation and Planning of a Magnetically
17 Actuated Microrobot Navigating in the Arteries, *IEEE Trans. BioMed. Eng.* 60
18 (2013) 994-1001.
- 19 [5] L. Arcese, M. Fruchard, A. Ferreira, Endovascular Magnetically Guided Robots:
20 Navigation Modeling and Optimization, *IEEE Trans. BioMed. Eng.* 59 (2012)
21 977-987.
- 22 [6] R. Blakemore, Magnetotactic Bacteria, *Science*, 190 (1975) 377-379.
- 23 [7] R.P. Blakemore, Magnetotactic bacteria, *Annu. Rev. Microbiol.* 36 (1982)
24 217-238.
- 25 [8] R.B. Frankel, D.A. Bazylinski, Magnetosomes and magneto-aerotaxis, *Contrib.*
26 *Microbiol.* 16 (2009) 182-193.
- 27 [9] D. Faivre, D. Schuler, Magnetotactic Bacteria and Magnetosomes, *Chem. Rev.*
28 108 (2008) 4875-4898.
- 29 [10] C.T. Lefevre, A. Bernadac, K. Yu-Zhang, N. Pradel, L.F. Wu, Isolation and
30 characterization of a magnetotactic bacterial culture from the Mediterranean Sea,
31 *Environmental microbiology*, 11 (2009) 1646-1657.
- 32 [11] R.B. Frankel, D.A. Bazylinski, M.S. Johnson, B.L. Taylor, Magneto-aerotaxis in
33 marine coccoid bacteria, *Biophys. J.* 73 (1997) 994-1000.
- 34 [12] M.M. Stanton, B.W. Park, D. Vilela, K. Bente, D. Faivre, M. Sitti, S. Sanchez,
35 Magnetotactic Bacteria Powered Biohybrids Target E. coli Biofilms, *ACS Nano.*
36 11 (2017) 9968-9978.
- 37 [13] S. Martel, C.C. Tremblay, S. Ngakeng, G. Langlois, Controlled manipulation and
38 actuation of micro-objects with magnetotactic bacteria, *Appl. Phys. Lett.* 89 (2006)

1 233904.

- 2 [14] Q. Ma, C. Chen, S. Wei, C. Chen, L.F. Wu, T. Song, Construction and operation
3 of a microrobot based on magnetotactic bacteria in a microfluidic chip,
4 *Biomicrofluidics*. 6 (2012) 24107-2410712.
- 5 [15] S.K. Alsaiari, A.H. Ezzedine, A.M. Abdallah, R. Sougrat, N.M. Khashab,
6 Magnetotactic bacterial cages as safe and smart gene delivery vehicles, *OpenNano*.
7 1 (2016) 36-45.
- 8 [16] S. Taherkhani, M. Mohammadi, J. Daoud, S. Martel, M. Tabrizian, Covalent
9 Binding of Nanoliposomes to the Surface of Magnetotactic Bacteria for the
10 Synthesis of Self-Propelled Therapeutic Agents, *ACS Nano*. 8 (2014) 5049-5060.
- 11 [17] O. Felfoul, M. Mohammadi, S. Taherkhani, D. de Lanauze, Y. Zhong Xu, D.
12 Loghin, S. Essa, S. Jancik, D. Houle, M. Lafleur, L. Gaboury, M. Tabrizian, N.
13 Kaou, M. Atkin, T. Vuong, G. Batist, N. Beauchemin, D. Radzioch, S. Martel,
14 Magneto-aerotactic bacteria deliver drug-containing nanoliposomes to tumour
15 hypoxic regions, *Nat. Nanotech*. 11 (2016) 941-947.
- 16 [18] L. Chen, C. Chen, P. Wang, C. Chen, L.-F. Wu, T. Song, A compound magnetic
17 field generating system for targeted killing of *Staphylococcus aureus* by
18 magnetotactic bacteria in a microfluidic chip, *J. Magn. Magn. Mater*. 427 (2017)
19 90-94.
- 20 [19] O. Felfoul, S. Martel, Assessment of navigation control strategy for
21 magnetotactic bacteria in microchannel: toward targeting solid tumors, *Biomed.*
22 *Microdevices*. 15 (2013) 1015-1024.
- 23 [20] D. Loghin, C. Tremblay, M. Mohammadi, S. Martel, Exploiting the responses of
24 magnetotactic bacteria robotic agents to enhance displacement control and swarm
25 formation for drug delivery platforms, *Int. J. Robot Res*. 36 (2017) 1195-1210.
- 26 [21] D. de Lanauze, O. Felfoul, J.-P. Turcot, M. Mohammadi, S. Martel,
27 Three-dimensional remote aggregation and steering of magnetotactic bacteria
28 microrobots for drug delivery applications, *Int. J. Robot Res*. 33 (2013) 359-374.
- 29 [22] E. Alphantery, F. Guyot, I. Chebbi, Preparation of chains of magnetosomes,
30 isolated from *Magnetospirillum magneticum* strain AMB-1 magnetotactic bacteria,
31 yielding efficient treatment of tumors using magnetic hyperthermia, *Int. J.*
32 *Pharmaceut*. 434 (2012) 444-452.
- 33 [23] C. Chen, L. Chen, Y. Yi, C. Chen, L.-F. Wu, T. Song, Killing of *Staphylococcus*
34 *aureus* via Magnetic Hyperthermia Mediated by Magnetotactic Bacteria, *Appl.*
35 *Environ. Microbiol*. 82 (2016) 2219-2226.
- 36 [24] C.Y. Chen, C.F. Chen, Y. Yi, L.J. Chen, L.F. Wu, T. Song, Construction of a
37 microrobot system using magnetotactic bacteria for the separation of
38 *Staphylococcus aureus*, *Biomed. Microdevices*. 16 (2014) 761-770.
- 39 [25] C. Chen, L. Chen, P. Wang, L.-F. Wu, T. Song, Magnetically-induced elimination
40 of *Staphylococcus aureus* by magnetotactic bacteria under a swing magnetic field,
41 *Nanomedicine: NBM*. 13 (2017) 363-370.
- 42 [26] I.S. Grant, W.R. Phillips, *Electromagnetism*, Wiley-Blackwell, London, 1975.
- 43 [27] C.S. Jürgen Rahmer, Bernhard Gleich, Spatially selective remote magnetic
44 actuation of identical helical micromachines, *Sci. Robot*. 2 (2017) eaal2845.

- 1 [28] F. El-Merhi, D. Garg, M. Cura, O. Ghaith, Peripheral vascular tumors and
2 vascular malformations: imaging (magnetic resonance imaging and conventional
3 angiography), pathologic correlation and treatment options, *Int. J. Cardiovas.*
4 *Imag.* 29 (2013) 379-393.
- 5 [29] W. Do, S.H. Choi, S. Park, Simultaneous Variable-Slab Dual-Echo TOF MR
6 Angiography and Susceptibility-Weighted Imaging, *IEEE Trans. Med. Imag.* 37
7 (2018) 1632-1640.
- 8 [30] J.H. Heo, K. Kim, J. Yoo, Y.D. Kim, H.S. Nam, E.Y. Kim, Computed
9 Tomography-Based Thrombus Imaging for the Prediction of Recanalization after
10 Reperfusion Therapy in Stroke, *J. Stroke.* 19 (2017) 40-49.
- 11 [31] C. Gillmann, T. Bauerle, Tumor Blood Vessel Visualization, *Meth. Mol. Biol.*
12 1464 (2016) 163-173.